

A new critical endpoint in thermomagnetic QCD

Mamiya Kawaguchi*

*Department of Physics and Center for Field Theory and Particle Physics,
Fudan University, 220 Handan Road, 200433 Shanghai, China*

Shinya Matsuzaki†

Center for Theoretical Physics and College of Physics, Jilin University, Changchun, 130012, China

Akio Tomiya‡

RIKEN BNL Research center, Brookhaven National Laboratory, Upton, NY, 11973, USA

A new critical endpoint is pinned down in the thermomagnetic-QCD phase structure, which is suggested to be present between the two-flavor and three-flavor massless limits. It is signaled by the electromagnetic scale anomaly in QCD, and is shown to be most eminent in a weak magnetic field regime, which is not well explored on lattice QCD.

PACS numbers:

The thermodynamical phase transition in quantum chromo-dynamics (QCD) is one of the crucial cosmological phase transitions in the thermal history of universe, hence needs to be well understood. Chiral symmetry then plays the key role and is essential in pursuing the QCD phase transition.

In reality, the chiral symmetry is explicitly broken by quark masses provided by coupling to the Higgs boson outside QCD. This explicit breaking keeps staying even in the thermal QCD at high temperatures, so would make the genuine chiral-phase transition nature obscure.

To reconcile this dilemma, it would be necessary to go away at the massless limit (so-called the chiral limit). There quarks enjoy the exact chiral symmetry. Accordingly, pions can be identified as the exactly massless Nambu-Goldstone bosons associated with the spontaneous breaking of the chiral symmetry. This chiral nature fully controls the low-energy description of QCD, hence allows addressing the chiral phase transition in the low-energy effective model, in spite of the intrinsic non-perturbative feature of low-energy QCD.

Indeed, Pisarski and Wilczek a long ago [1] paid their particular attention to the chiral limit, off the physical point, and employed an effective model in the confinement phase based on the exact chiral symmetry with or without $U(1)$ axial symmetry. They discussed existence of the renormalization group-fixed point, to suggest that the order of the chiral phase transition highly depends on the number of massless flavors. This was the pioneering work and made a significant help to comprehend QCD at the physical point as the chiral theory.

Columbia university group extended their work using lattice QCD calculations [2]. In lattice QCD, mass and the number of flavor dependence on the order of the QCD

phase transition have been investigated including the chiral and confinement-deconfinement phase transitions. It is summarized as what is called Columbia plot.

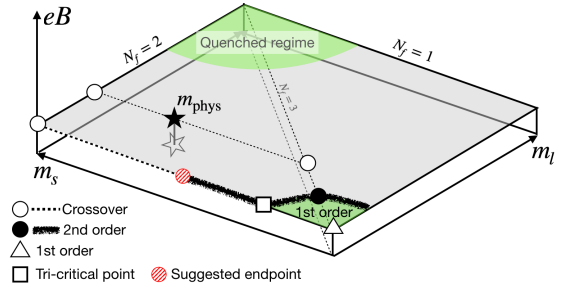


FIG. 1: Extended Columbia plot along with an external magnetic field in the weak field regime. m_l and m_s denote masses of the light quarks and strange quark, respectively. Our suggested endpoint is indicated by a shaded circle. A blank square stands for the tri-critical point, at which the three domains of crossover, first- and second-order phase transitions merge. The details are described in the text. Another second order point we have found is denoted as the black circular blob at $m_\pi < m_{\text{phys}}$. For details, see Appendix F. The physical point is known to be the crossover [3] at this size of magnetic field.

Since the early work of Columbia group used an approximated algorithm, it has nowadays been refined by utilizing modern technologies. In the two flavor chiral limit and 2+1 flavor chiral limit, namely with two of massless quarks and one heavy quark, restoration or persistence of $U(1)$ axial anomaly above the critical temperature has been discussed [4–11]. It is shown that restoration or persistence is tightly connected to the order of phase transition and its universality class [1, 12–14]. On

*kawaguchi@fudan.edu.cn

†synya@jlu.edu.cn

‡akio.tomiya@riken.jp

the other hand, QCD is believed to exhibit the first-order phase-transition in the three-flavor chiral limit [1]. However, no clear lattice results for the first-order phase-transition has been obtained and only lower limits on the quark mass in the crossover has been placed [15, 16].

Current targets for lattice QCD have been extended including a constant magnetic field. Such magnetized QCD has terrestrially been created by so-called the “little bang” in the early stage of non-central collisions in relativistic heavy ion experiments. Lots of interesting results have been reported from lattice studies on the QCD thermodynamics in the strong external magnetic field [17–20]. Of these results, there are two striking properties discovered: the reduction of transition temperature [21–25] and the inverse magnetic catalysis [3].

In contrast, the weak magnetic field has not fully been investigated on the lattice QCD. At the current status, the smallest nonzero magnetic field on the lattice is $\sqrt{eB}_{\min} \sim 0.1$ GeV [3], which is only for the physical pion mass simulations. This is because of the fact that the minimal magnetic field is determined by the area of transverse plane to the magnetic field [3]. Thus the weak magnetic field with smaller pion masses, particularly close to the chiral limit, is challenging due to the higher numerical cost.

Instead of lattices, chiral effective theories would therefore shed light on the weak magnetic regime at the chiral limit, as if it gets back to the epoch where the Columbia plot was first proposed along the pioneering work by Pisarski and Wilczek.

In this Letter, we pave a way to investigate the chiral phase transition at the chiral limit in a weakly magnetized QCD. Based on a chiral effective model inspired by Pisarski and Wilczek, we find that there is a new critical endpoint between the massless two- and three-flavor chiral limits. It is shown that this new phase transition is triggered essentially due to the electromagnetic scale anomaly in QCD, which gets most eminent in the weak magnetic field regime.

Our current analysis is based on an effective potential approach, not on the renormalization group method like in the Pisarski and Wilczek’s work. Cross-check using the (nonperturbative) renormalization group would make our finding more evident, which will be pursued elsewhere.

The proposed critical endpoint is marked as “Suggested endpoint”, in an extended Columbia plot including the magnetic field in the weak field regime ^{#1}, Fig. 1. This is our main result in the present paper.

Before entering the detailed demonstration, we shall present an intuitive interpretation on the chiral phase transition nature, which would help readers to easily

grasp our new finding. To this end, we momentarily work on a generic Ginzburg-Landau description for the chiral phase transition.

In the Ginzburg-Landau approach, the chiral phase structure can be described by a generic effective potential in terms of the order parameter $\bar{\sigma}_0$. It takes the polynomial form

$$V_{\text{eff}}(\bar{\sigma}_0) = \alpha_1(T, eB)\bar{\sigma}_0 + \alpha_2(T, eB)\bar{\sigma}_0^2 + \alpha_3(T, eB)\bar{\sigma}_0^3 + \alpha_4(T, eB)\bar{\sigma}_0^4 + \dots \quad (1)$$

where the potential parameters $\alpha_{i=1,2,3,4,\dots}$ can include intrinsic temperature- and/or magnetic-dependence. Our sigma field is defined as an interpolating mesonic degree of freedom for the lightest quark bilinear $\bar{q}q$ in QCD.

When the exact chiral symmetry is imposed, the effective potential form is restricted to be an even function of $\bar{\sigma}_0$, such as $\bar{\sigma}_0^2$ and $\bar{\sigma}_0^4$. With terms truncated up to $O(\bar{\sigma}_0^4)$, the phase transition is then expected to be of the second order.

In the three-flavor case, the $U(1)$ axial anomaly induces the cubic term of $\bar{\sigma}_0$, which originally takes a determinant form of the quark condensate, $\det\bar{q}q \sim \bar{\sigma}_0^3$, a la Kobayashi-Maskawa-’t Hooft [28–31]. Then, the phase transition order is changed to be of the first order, because the cubic term creates a potential barrier between the chiral symmetric vacuum ($\bar{\sigma}_0 = 0$) and broken one ($\bar{\sigma}_0 \neq 0$). Note here that the determinant term in the two-flavor case can be absorbed into $\bar{\sigma}_0^2$ term, due to the speciality of the $SU(2)$ group, so the $U(1)$ axial anomaly does not effectively affect the potential form.

As to the linear (tadpole) term of $\bar{\sigma}_0$, it cannot be present even with the $U(1)$ axial anomaly. It would show up when the current quark masses are introduced, which can explicitly break the full chiral symmetry including the $U(1)$ axial part. Once the tadpole is present, the potential no longer achieves the exactly chiral symmetric vacuum, which, in other words, the theory always lies in the broken phase, even though the value of $\bar{\sigma}_0$ gets smaller, as T becomes higher. This implies that the tadpole term in the potential drives the phase transition to be continuous, i.e., crossover, called the chiral crossover.

Below, we will observe that a tadpole term is generated even for the massless flavor case, in the thermomagnetic QCD. The phase transition becomes crossover, so there should be a critical endpoint seen in the interplay between massless two-flavor and three-flavor thermomagnetic QCD, as in Fig. 1.

Of crucial is to note that the sigma field serves as a source for the scale anomaly in QCD, which includes the magnetic field contribution in the thermomagnetic QCD. This provides a tadpole term for the sigma field in the effective potential. The coupling form between the sigma field and the scale anomaly can unambiguously be determined by the Ward-Takahashi identity for the anomalous scale symmetry. The coupling separately includes the vacuum part and the thermomagnetic correction part, both of which arise from quark loops coupled to the sigma

^{#1} Other critical points have been proposed in a strong magnetic field regime [26, 27]. Our finding is definitely different from those which are expected to emerge due to broadening of the quenched regime in Fig. 1 because of the amplified mass gap of quarks by the strong magnetic field.

field. The vacuum part comes along with the electromagnetic field strength, while the thermomagnetic part with the thermal mass of the electromagnetic field. The details are given in Appendices B, C, D, and E. Note here that both of two electromagnetic-scale anomaly terms take the form of the transverse polarization, following the electromagnetic gauge invariance. Therefore, they will tend to vanish as the magnetic field gets strong enough, because the dynamics of quarks are governed by the lowest Landau level states polarized along the direction parallel to the magnetic field. Thus, the electromagnetic scale anomaly will be most eminent in a weak magnetic regime.

To explicitly see what form the tadpole takes, we employ a quark-meson model in a constant weak magnetic field #². The model description is detailed in Appendices A and E. The tadpole term is thus generated in the effective potential of $\bar{\sigma}_0$ as

$$V_{\text{eff}}^{(\text{Tad})}(\bar{\sigma}_0) = -\sqrt{\frac{2}{N_f}} \frac{\bar{\sigma}_0}{f_\pi} \left[\frac{\beta(e)}{e} B^2 + \frac{1}{2e^2} \sum_f Q_f^2 F(T, m_{\text{dyn}}) eB \right]. \quad (2)$$

This tadpole arises even in the chiral limit, as the magnetically induced-explicit chiral-breaking effect. Here f_π is the pion decay constant at vacuum; e denotes the electromagnetic coupling; eB is the constant magnetic field strength; Q_f with $f = u, d$ (and s) is the electromagnetic charge for quark flavor f . The vacuum contribution (the first term) comes along with the beta function of e , $\beta(e)$, which we evaluate at the one-loop level, $\beta(e) = \frac{e^3}{(4\pi)^2} \frac{4N_c}{3} \sum_f Q_f^2$, with $N_c = 3$. $F(T, m_{\text{dyn}})$ is a thermal one-loop function depending on T and the dynamical quark mass m_{dyn} which is generated in the quark-meson model (See Appendices C, D, and E).

In addition to the induced tadpole in Eq.(2), the sigma potential involves several terms generated from the thermomagnetic dynamics. For simplicity, as in the literature, we may work in the large N_c limit, and only take into account the quark loops at one-loop level. The resultant explicit form of the effective potential (V_{eff}), as well as its derivation, and the way of fixing the potential parameters are given in Appendices A, D and E.

Two plots in Fig. 2 exhibit a sketch of the thermomagnetic phase transition for the chiral $SU(2)_L \times SU(2)_R$ symmetry based on the quark-meson model with massless two flavors. As clearly seen, the scale-anomaly induced-tadpole term in Eq.(2) makes the phase transition crossover, in somewhat a weak magnetic regime less

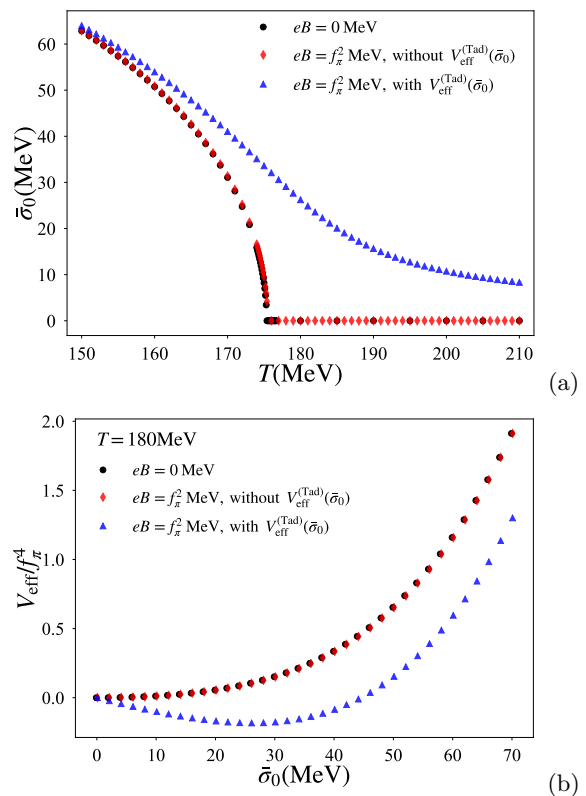


FIG. 2: The chiral phase transition for massless two-flavor case, predicted from the quark-meson model in the large N_c limit. The panel (a) shows the T -dependence of the chiral order parameter $\bar{\sigma}_0$, around the critical temperature $T_c \simeq 175$ MeV. The panel (b) displays the deformation of the effective potential V_{eff} , normalized to the (fourth power of) pion decay constant f_π ($\simeq 93$ MeV) at vacuum. The effective potential has been normalized by subtracting $V_{\text{eff}}(\bar{\sigma}_0 = 0)$ at $T = 180$ MeV. Both panels monitor the eB dependence in unit of f_π^2 , for two cases with or without the scale anomaly-induced tadpole term included.

than the (square of) chiral critical temperature $T_c \simeq 175$ MeV (for $eB = 0$) #³. This puts the milestone marked as “Crossover” at the crossed point in the eB axis at $m_s \rightarrow \infty$, in the extended Columbia plot in Fig. 1.

Turning to the massless three-flavor case, we make similar plots in Fig. 3. In this case, the chiral phase transition for the $SU(3)_L \times SU(3)_R$ symmetry is still of the first order, even the presence of the induced tadpole, though the chiral order parameter cannot exactly reach zero because of the tadpole. This is essentially due to the sizable $U(1)$ axial anomaly contribution generating the cubic po-

#² It has been discussed [32, 33] that in a strong magnetic field regime, the quark-meson model can reproduce the reduction of the (pseudo) critical temperature of the chiral crossover and the inverse magnetic catalysis for the quark condensate, discovered on the lattice [3, 21–25].

#³ The value of T_c estimated from the present quark-meson model does not agree with the result with the chiral extrapolation (only applied to the lightest two-flavors) on the lattice QCD with 2+1 flavors, $T_{c|\text{lat.}} = 132^{+3}_{-6}$ MeV [10]. However, this quantitative discrepancy is irrespective of our main claim in Fig. 1.

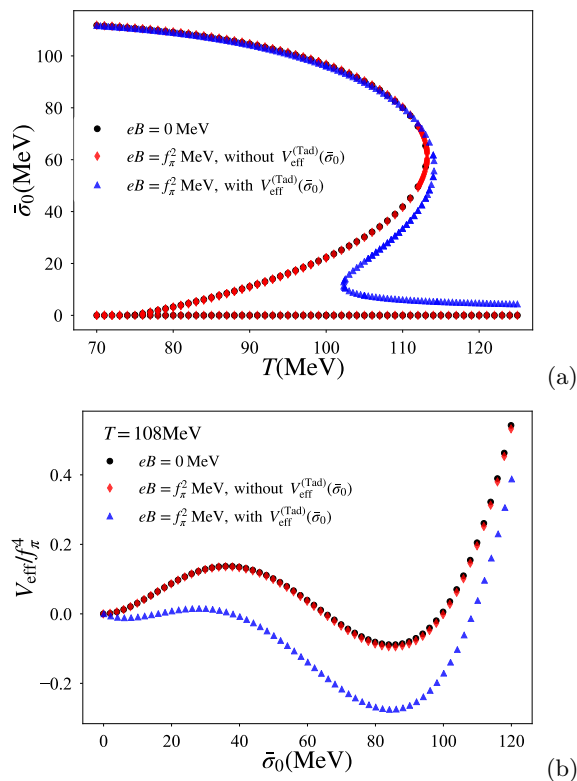


FIG. 3: The same as Fig. 2, but for massless three flavors. The chiral critical temperature at $eB = 0$ is $T_c = 113$ MeV. The effective potential V_{eff} has been normalized in the same way as in Fig. 2, and subtracted by the value at $\bar{\sigma}_0 = 0$ evaluated at $T = 108$ MeV.

tential term, as evaporated in the Ginzburg-Landau description around Eq.(1) ^{#4}. This result is marked as “1st order” in the extended Columbia plot, in Fig. 1.

Thus, combining the explicit results in Figs 2 and 3, we can conclude that in the extended Columbia plot, along the m_s axis, there should be a critical endpoint marked as a second order phase transition – that is the “Suggested endpoint”, in Fig. 1.

See Fig. 1. One interesting question is whether or not the second order nature persists when m_s gets smaller along the m_s axis.

If it does, there should be a second-order phase transition line on the m_s axis, extended from the suggested endpoint down to the first-order phase transition domain surrounded by the observed first-order point in Fig. 3. This is illustrated as the black-bold line on the m_s axis,

^{#4} It has been noted in the literature [34] that at $T < 1.5T_c$ the instanton effects are not significantly suppressed. In terms of the present quark-meson model, this implies that the corresponding coupling (B_{anom} in Eq.(A6)) for the $U(1)$ -axial anomaly term, giving the $\alpha_3(T, eB)\bar{\sigma}_0^3$ term in Eq.(1), can still be effective over the possible thermal suppression at around $T = T_c$.

in Fig. 1. Here one should notice that there should also be a tri-critical point, at which the three phases (first, second, and crossover domains) overlap. It is marked by a blank square, in Fig. 1. In that case, existence of the second-order phase transition line might be interpreted a remnant of the universality class of $O(4)$ on the m_s axis, as in the Columbia plot without magnetic field [2].

If the crossover nature, confirmed at $m_s \rightarrow \infty$ in Fig. 2, keeps until the first-order phase transition domain surrounded by the observed first-order point in Fig. 3, the tri-critical point will no longer be the one: the tri-critical point is *eaten* and replaced by the new critical endpoint, due to the electromagnetic-scale anomaly *pollution* spoiling the second order phase transition nature.

At any rate, searching for the new critical endpoint is of importance, and paves the way to this new frontier in the extended Columbia plot, Fig. 1.

In conclusion, a new critical endpoint has been pinned down in the thermomagnetic-QCD phase structure, which is located between the massless two-flavor and three-flavor limits (displayed in the extended Columbia plot, Fig. 1, marked as the “Suggested endpoint”). This is shown to be signaled by the electromagnetic scale anomaly in QCD, and most eminent in a weak magnetic field regime.

Currently, the chiral-extrapolation on lattice in absence of a magnetic field has extensively been systematically studied, and improved so much in the case with $2 + 1$ flavors [10]. On the other hand, there has been remarkable progress on creating small magnetic fields at the physical point, and the current lower bound is ~ 100 MeV [3]. Therefore, it is highly anticipated that the new critical endpoint is accessible to search on lattice QCD in near future.

More on thermodynamical properties in thermomagnetic QCD with the electromagnetic scale anomaly will be pursued in another publication. It is also worth cross-checking our finding by the (nonperturbative) renormalization group method.

The presently proposed new critical endpoint is off the physical point. Extension by including a finite baryon chemical potential (μ_B) might kick it up at the physical point, analogously to the prospected existence of the QCD critical endpoint in the conventional QCD phase diagram on the $\mu_B - T$ plane: the existence of the QCD critical endpoint can be understood by a simple extrapolation of the three-flavor chiral limit on the Columbia plot [35]. Investigation along this possibility would also be worth pursuing.

Our finding would also be relevant to modeling magnetized thermal QCD-like theories beyond the standard model of particle physics. For instance, it would impact gravitational wave productions addressed by a chiral phase transition in a dark/hidden QCD theory with three flavors together with a magnetic field weaker than the target QCD scale, which originates from redshifting the primordially produced one. Having one heavier flavor among three would be incompatible and cannot realize

the first-order phase transition desired to create sources of gravitational waves.

This work was supported in part by the National Science Foundation of China (NSFC) under Grant

No.11747308, 11975108, 12047569, and the Seeds Funding of Jilin University (S.M.). The work of A.T. was supported by the RIKEN Special Postdoctoral Researcher program and partially by JSPS KAKENHI Grant Number JP20K14479.

-
- [1] Robert D. Pisarski and Frank Wilczek. Remarks on the chiral phase transition in chromodynamics. *Phys. Rev. D*, 29:338–341, Jan 1984.
- [2] Frank R. Brown, Frank P. Butler, Hong Chen, Norman H. Christ, Zhihua Dong, Wendy Schaffer, Leo I. Unger, and Alessandro Vaccarino. On the existence of a phase transition for qcd with three light quarks. *Phys. Rev. Lett.*, 65:2491–2494, Nov 1990.
- [3] G. S. Bali, F. Bruckmann, G. Endrodi, Z. Fodor, S. D. Katz, S. Krieg, A. Schafer, and K. K. Szabo. The QCD phase diagram for external magnetic fields. *JHEP*, 02:044, 2012.
- [4] Guido Cossu, Sinya Aoki, Hidenori Fukaya, Shoji Hashimoto, Takashi Kaneko, Hideo Matsufuru, and Jun-ichi Noaki. Finite temperature study of the axial $u(1)$ symmetry on the lattice with overlap fermion formulation. *Phys. Rev. D*, 87:114514, Jun 2013.
- [5] A. Tomiya, G. Cossu, S. Aoki, H. Fukaya, S. Hashimoto, T. Kaneko, and J. Noaki. Evidence of effective axial $u(1)$ symmetry restoration at high temperature qcd. *Phys. Rev. D*, 96:034509, Aug 2017.
- [6] S. Aoki, Y. Aoki, G. Cossu, H. Fukaya, S. Hashimoto, T. Kaneko, C. Rohrhofer, and K. Suzuki. Study of axial $U(1)$ anomaly at high temperature with lattice chiral fermions. 11 2020.
- [7] A. Bazavov, Tanmoy Bhattacharya, Michael I. Buchoff, Michael Cheng, N. H. Christ, H.-T. Ding, Rajan Gupta, Prasad Hegde, Chulwoo Jung, F. Karsch, Zhongjie Lin, R. D. Mawhinney, Swagato Mukherjee, P. Petreczky, R. A. Soltz, P. M. Vranas, and Hantao Yin. Chiral transition and $u(1)_A$ symmetry restoration from lattice qcd using domain wall fermions. *Phys. Rev. D*, 86:094503, Nov 2012.
- [8] Michael I. Buchoff, Michael Cheng, Norman H. Christ, H.-T. Ding, Chulwoo Jung, F. Karsch, Zhongjie Lin, R. D. Mawhinney, Swagato Mukherjee, P. Petreczky, Dwight Renfrew, Chris Schroeder, P. M. Vranas, and Hantao Yin. Qcd chiral transition, $u(1)_A$ symmetry and the dirac spectrum using domain wall fermions. *Phys. Rev. D*, 89:054514, Mar 2014.
- [9] Tanmoy Bhattacharya, Michael I. Buchoff, Norman H. Christ, H.-T. Ding, Rajan Gupta, Chulwoo Jung, F. Karsch, Zhongjie Lin, R. D. Mawhinney, Greg McGlynn, Swagato Mukherjee, David Murphy, P. Petreczky, Dwight Renfrew, Chris Schroeder, R. A. Soltz, P. M. Vranas, and Hantao Yin. Qcd phase transition with chiral quarks and physical quark masses. *Phys. Rev. Lett.*, 113:082001, Aug 2014.
- [10] H.-T. Ding, P. Hegde, O. Kaczmarek, F. Karsch, Anirban Lahiri, S.-T. Li, Swagato Mukherjee, H. Ohno, P. Petreczky, C. Schmidt, and P. Steinbrecher. Chiral phase transition temperature in $(2+1)$ -flavor qcd. *Phys. Rev. Lett.*, 123:062002, Aug 2019.
- [11] H. T. Ding, S. T. Li, Swagato Mukherjee, A. Tomiya, X. D. Wang, and Y. Zhang. Correlated Dirac eigenvalues and axial anomaly in chiral symmetric QCD. 10 2020.
- [12] Sinya Aoki, Hidenori Fukaya, and Yusuke Taniguchi. Chiral symmetry restoration, the eigenvalue density of the dirac operator, and the axial $u(1)$ anomaly at finite temperature. *Phys. Rev. D*, 86:114512, Dec 2012.
- [13] Tomomi Sato and Norikazu Yamada. Linking $u(2) \times u(2)$ to $o(4)$ model via decoupling. *Phys. Rev. D*, 91:034025, Feb 2015.
- [14] Yu Nakayama and Tomoki Ohtsuki. Bootstrapping phase transitions in qcd and frustrated spin systems. *Phys. Rev. D*, 91:021901, Jan 2015.
- [15] A. Bazavov, H.-T. Ding, P. Hegde, F. Karsch, E. Laermann, Swagato Mukherjee, P. Petreczky, and C. Schmidt. Chiral phase structure of three flavor qcd at vanishing baryon number density. *Phys. Rev. D*, 95:074505, Apr 2017.
- [16] Xiao-Yong Jin, Yoshinobu Kuramashi, Yoshifumi Nakamura, Shinji Takeda, and Akira Ukawa. Critical point phase transition for finite temperature 3-flavor qcd with nonperturbatively $O(a)$ improved wilson fermions at $N_t = 10$. *Phys. Rev. D*, 96:034523, Aug 2017.
- [17] Dmitri E. Kharzeev, Larry D. McLerran, and Harmen J. Warringa. The Effects of topological charge change in heavy ion collisions: 'Event by event P and CP violation'. *Nucl. Phys. A*, 803:227–253, 2008.
- [18] Massimo D'Elia. Lattice QCD Simulations in External Background Fields. *Lect. Notes Phys.*, 871:181–208, 2013.
- [19] D. E. Kharzeev, J. Liao, S. A. Voloshin, and G. Wang. Chiral magnetic and vortical effects in high-energy nuclear collisions—A status report. *Prog. Part. Nucl. Phys.*, 88:1–28, 2016.
- [20] Gergely Endrödi. QCD in magnetic fields: from Hofstadter's butterfly to the phase diagram. *PoS, LATTICE2014:018*, 2014.
- [21] V. G. Bornyakov, P. V. Buividovich, N. Cundy, O. A. Kochetkov, and A. Schäfer. Deconfinement transition in two-flavor lattice qcd with dynamical overlap fermions in an external magnetic field. *Phys. Rev. D*, 90:034501, Aug 2014.
- [22] G. S. Bali, F. Bruckmann, G. Endrödi, S. D. Katz, and A. Schäfer. The QCD equation of state in background magnetic fields. *JHEP*, 08:177, 2014.
- [23] Akio Tomiya, Heng-Tong Ding, Xiao-Dan Wang, Yu Zhang, Swagato Mukherjee, and Christian Schmidt. Phase structure of three flavor QCD in external magnetic fields using HISQ fermions. *PoS, LATTICE2018:163*, 2019.
- [24] Massimo D'Elia, Floriano Manigrasso, Francesco Negro, and Francesco Sanfilippo. QCD phase diagram in a magnetic background for different values of the pion mass. *Phys. Rev. D*, 98(5):054509, 2018.
- [25] Gergely Endrodi, Matteo Giordano, Sandor D. Katz,

- T. G. Kovács, and Ferenc Pittler. Magnetic catalysis and inverse catalysis for heavy pions. *JHEP*, 07:007, 2019.
- [26] Thomas D. Cohen and Naoki Yamamoto. New critical point for QCD in a magnetic field. *Phys. Rev. D*, 89(5):054029, 2014.
- [27] Gergely Endrodi. Critical point in the QCD phase diagram for extremely strong background magnetic fields. *JHEP*, 07:173, 2015.
- [28] M. Kobayashi and T. Maskawa. Chiral symmetry and eta-x mixing. *Prog. Theor. Phys.*, 44:1422–1424, 1970.
- [29] M. Kobayashi, H. Kondo, and T. Maskawa. Symmetry breaking of the chiral $u(3) \times u(3)$ and the quark model. *Prog. Theor. Phys.*, 45:1955–1959, 1971.
- [30] Gerard 't Hooft. Symmetry Breaking Through Bell-Jackiw Anomalies. *Phys. Rev. Lett.*, 37:8–11, 1976.
- [31] Gerard 't Hooft. Computation of the Quantum Effects Due to a Four-Dimensional Pseudoparticle. *Phys. Rev. D*, 14:3432–3450, 1976. [Erratum: *Phys.Rev.D* 18, 2199 (1978)].
- [32] Alejandro Ayala, M. Loewe, and R. Zamora. Inverse magnetic catalysis in the linear sigma model with quarks. *Phys. Rev. D*, 91(1):016002, 2015.
- [33] Jens O. Andersen, William R. Naylor, and Anders Tranberg. Inverse magnetic catalysis and regularization in the quark-meson model. *JHEP*, 02:042, 2015.
- [34] Robert D. Pisarski and Fabian Rennecke. Multi-instanton contributions to anomalous quark interactions. *Phys. Rev. D*, 101(11):114019, 2020.
- [35] Philippe de Forcrand and Massimo D'Elia. Continuum limit and universality of the Columbia plot. *PoS, LAT-TICE2016:081*, 2017.
- [36] Jens O. Andersen and Rashid Khan. Chiral transition in a magnetic field and at finite baryon density. *Phys. Rev. D*, 85:065026, 2012.
- [37] Muneyuki Ishida. Possible classification of the chiral scalar sigma nonet. *Prog. Theor. Phys.*, 101:661–669, 1999.
- [38] Yoshiki Kuroda, Masayasu Harada, Shinya Matsuzaki, and Daisuke Jido. Inverse Mass Hierarchy of Light Scalar Mesons Driven by Anomaly-Induced Flavor Breaking. *PTEP*, 2020(5):053D02, 2020.
- [39] H. Arthur Weldon. Covariant Calculations at Finite Temperature: The Relativistic Plasma. *Phys. Rev. D*, 26:1394, 1982.
- [40] K. Ahmed and S. S. Masood. Vacuum polarization at finite temperature and density in QED. *Annals Phys.*, 207:460–473, 1991.

Appendix A: Ginzburg-Landau description based on linear sigma model approach

From the viewpoint of the low-energy hadron dynamics for N_f -flavor QCD, the chiral phase transition can be described by the Ginzburg-Landau approach based on the linear sigma model. Here we derive the mode potential.

First of all, we introduce the building block, the linear sigma model field Φ , which is parametrized by the scalar- and pseudoscalar-meson fields as

$$\Phi = \begin{cases} \frac{1}{2}(\sigma_0 + i\tau^i \pi^i), & (\text{for } N_f = 2) \\ \frac{1}{2}(\sigma_a + i\pi_a)\lambda^a, & (\text{for } N_f = 3), \end{cases} \quad (\text{A1})$$

where $\tau_{i=1,\dots,3}$ are the Pauli matrices and $\lambda_{a=1,\dots,8}$ represent the Gell-Mann matrices with $\lambda_0 = \sqrt{2/3} \cdot \mathbf{1}_{3 \times 3}$. Under the chiral symmetry we define the transformation law of Φ as

$$\Phi \rightarrow \begin{cases} g_L \cdot \Phi \cdot g_R^\dagger, & (\text{for } N_f = 2) \\ g_A \cdot g_L \cdot \Phi \cdot g_R^\dagger, & (\text{for } N_f = 3), \end{cases} \quad (\text{A2})$$

where $g_{L,R} \in SU(2)_{L,R}$ in the case of $N_f = 2$, and $g_{L,R} \in SU(3)_{L,R}$ with $g_A \in U(1)_A$ in the case of $N_f = 3$.

Thus the linear sigma model is constructed based on the chiral invariance with its breaking source, including operators up to dimension four, as

$$\mathcal{L}_{\text{LSM}} = \text{tr} [\partial_\mu \Phi \partial^\mu \Phi^\dagger] - V(\Phi), \quad (\text{A3})$$

where $V(\Phi)$ represents the potential terms,

$$V(\Phi) = V_0(\Phi) + V_{\text{anom}}(\Phi) + V_{\text{SB}}(\Phi). \quad (\text{A4})$$

In Eq.(A4) $V_0(\Phi)$ is the chiral invariant part:

$$V_0(\Phi) = \mu^2 \text{tr}[(\Phi^\dagger \Phi)] + \lambda_1 \text{tr}[(\Phi^\dagger \Phi)^2] + \lambda_2 (\text{tr}[(\Phi^\dagger \Phi)])^2, \quad (\text{A5})$$

where μ^2 is the mass parameter taken either a positive or negative value. $\lambda_{1,2}$ are dimensionless quartic coupling constants, which cannot be taken independently in the case of $N_f = 2$, because of the speciality of $SU(2)$ algebra.

For $N_f = 3$, the $U(1)$ axial anomalous part, but keeping the chiral $SU(N_f)_L \times SU(N_f)_R$ symmetry, represents $V_{\text{anom}}(\Phi)$. The lowest dimensional operator for the $U(1)$ axial anomalous part is given by a la Kobayashi-Maskawa-'t Hooft [28–31],

$$V_{\text{anom}}(\Phi) = -B_{\text{anom}} (\det[\Phi] + \det[\Phi^\dagger]), \quad (\text{A6})$$

where the parameter B_{anom} is taken to be real, which has mass dimension one.

In the case of $N_f = 2$, V_{anom} can be absorbed into the μ^2 terms, again, because of the speciality of the $SU(2)$ algebra.

In the underlying QCD Lagrangian, the chiral symmetry is explicitly broken by the current quark mass matrix $\mathcal{M} = \text{diag}\{m_u, m_d, m_s\}$. In the linear-sigma model-Lagrangian, this explicit breaking effect is reflected in the V_{SB} part:

$$V_{\text{SB}}(\Phi) = -c \text{tr}[\mathcal{M}\Phi^\dagger + \mathcal{M}^\dagger \Phi], \quad (\text{A7})$$

where the parameter c is taken to be a real value, and has mass dimension two.

To be consistent with the underlying QCD, we choose the vacuum expectation value of the Φ field to respect the vectorial symmetry, $SU(2)_V$ or $SU(3)_V$, in such a way that

$$\langle \Phi \rangle = \bar{\Phi} \cdot \mathbf{1} = \begin{cases} \frac{1}{2}\bar{\sigma}_0 \cdot \mathbf{1}_{2 \times 2}, & (\text{for } N_f = 2) \\ \frac{1}{2}\sqrt{\frac{2}{3}}\bar{\sigma}_0 \cdot \mathbf{1}_{3 \times 3}, & (\text{for } N_f = 3). \end{cases} \quad (\text{A8})$$

Thus the linear sigma model potential can be viewed as a Ginzburg-Landau description, at the tree level (i.e. mean field level):

$$V_{\text{tree}}(\bar{\sigma}_0) = \begin{cases} -\sum_f c m_f \bar{\sigma}_0 + \frac{1}{2}(\mu^2 - B_{\text{anom}})\bar{\sigma}_0^2 + (\frac{\lambda_1}{8} + \frac{\lambda_2}{4})\bar{\sigma}_0^4, & (\text{for } N_f = 2) \\ -\sqrt{\frac{2}{3}}\sum_f c m_f \bar{\sigma}_0 + \frac{1}{2}\mu^2 \bar{\sigma}_0^2 - \frac{B_{\text{anom}}}{3\sqrt{6}}\bar{\sigma}_0^3 + (\frac{\lambda_1}{12} + \frac{\lambda_2}{4})\bar{\sigma}_0^4, & (\text{for } N_f = 3). \end{cases} \quad (\text{A9})$$

From this potential, the expectation value $\bar{\sigma}_0$ can be determined from the stationary condition,

$$\frac{\partial V_{\text{eff}}(\bar{\sigma}_0)}{\partial \bar{\sigma}_0} = 0. \quad (\text{A10})$$

At the tree level evaluation, it is related to the pion decay constant f_π as

$$f_\pi = 2\bar{\Phi}. \quad (\text{A11})$$

We can also discuss the order of chiral phase transition from the tree-level potential in Eq. (A9). At the chiral limit for the case of $N_f = 2$ ($m_f = 0$), the parameter B_{anom} can be absorbed in the mass parameter μ^2 , so that the $U(1)$ axial anomaly part does not effectively affect the order of chiral phase transition. The tree-level potential then has only the $\bar{\sigma}_0^2$ and $\bar{\sigma}_0^4$ terms. Thus, in the massless two-flavor case, the phase transition is deduced to be of the second order.

In the massless three-flavor case, the $U(1)$ axial anomaly part generates the cubic term of $\bar{\sigma}_0$, which creates a potential barrier between the chiral symmetric vacuum ($\bar{\sigma}_0 = 0$) and broken one ($\bar{\sigma}_0 \neq 0$). In association with the deformation of the potential, the phase transition is changed to be of the first order.

The meson masses can also be evaluated in the linear sigma model. Even when coupled to quarks so that the model is extended to the quark-meson model, the mass formulae at the tree-level will still be available in the large N_c limit, where only the quark loop effects are taken into account.

For the two-flavor case, the meson masses are given as

$$\begin{aligned} m_\pi^2 &= \mu^2 + \frac{1}{2}\lambda_1 f_\pi^2 \\ &= \sum_f c m_f \frac{1}{f_\pi}, \\ m_\sigma^2 &= \mu^2 + \frac{3}{2}\lambda_1 f_\pi^2. \end{aligned} \quad (\text{A12})$$

Here, we have used the stationary condition in Eq.(A10). In addition, $B(\lambda_2)$ has been absorbed into $\mu^2(\lambda_1)$, as noted above. In the chiral limit ($m_f \rightarrow 0$), the pion mass m_π goes to zero. To implement the numerical calculation in the present paper for the two-flavor chiral limit, we have set $m_\sigma = 800$ MeV, just for a reference value as in the literature [33, 36].

For the three-flavor case, meson masses are given as

$$\begin{aligned} m_\pi^2 &= \sum_f c m_f \sqrt{\frac{2}{3}} \frac{1}{f_\pi} \\ m_\sigma^2 &= \mu^2 - B_{\text{anom}} f_\pi + \frac{3}{2}(\lambda_1 + 3\lambda_2) f_\pi^2. \\ m_{\eta'}^2 &= m_\pi^2 + \frac{3}{2} B_{\text{anom}} f_\pi \\ m_{a_0}^2 &= \frac{2}{3} m_{\eta'}^2 + \frac{1}{3} m_\pi^2 + \lambda_1 f_\pi^2 \\ &= m_\sigma^2 + m_{\eta'}^2 - m_\pi^2 - 3\lambda_2 f_\pi^2. \end{aligned} \quad (\text{A13})$$

For the three-flavor chiral limit analysis, meson masses have been fixed to $m_\sigma = 650$ MeV, $m_{a_0} = 940$ MeV, and $m_{\eta'} = 960$ MeV, which are typical values obtained in the framework of linear sigma models [37, 38].

Appendix B: A general low energy theorem for scale symmetry

In the low-energy meson-dynamics, the scalar meson fields serve as a source for the scale symmetry breaking in QCD, accompanied with the chiral symmetry breaking. In the scale (dilatation) current, the lightest isosinglet scalar will govern, which would be identified as the signal particle for the spontaneous chiral symmetry breaking. Then, in a low-energy regime, the lightest isosinglet scalar can only couple to the dilatation current j_D^μ , and it is generally expressed as the overlap amplitude, like

$$\langle 0 | \partial_\mu j_D^\mu(x) | \sigma_0(p) \rangle = \langle 0 | (T^\mu{}_\mu)_{\text{meson}}(x) | \sigma_0(p) \rangle = \bar{\sigma}_0 m_\sigma^2 e^{-ip \cdot x}, \quad (\text{B1})$$

where $(T^\mu_\mu)_{\text{meson}}$ is the trace of the energy momentum tensor described by mesons. The overall sign would be minus, and then it can be absorbed in the pion decay constant (or redefinition of the $\bar{\sigma}_0$ field). Equation (B1) can be thought of as a low energy theorem for the scale symmetry. One can easily check that the linear sigma model surely reproduces the low energy theorem in Eq. (B1), in such a way that

$$\begin{aligned} \partial_\mu j_D^\mu &= (T^\mu_\mu)_{\text{meson}} = 2\mu^2 \text{tr}[\Phi^\dagger \Phi] + (N_f - 4)B(\det\Phi + \det\Phi^\dagger) - 3\text{ctr}[\mathcal{M}\Phi^\dagger + \mathcal{M}^\dagger\Phi], \\ \rightarrow \langle 0 | (T^\mu_\mu)_{\text{meson}}(x) | \sigma_0(p) \rangle &= \sqrt{\frac{N_f}{2}} f_\pi m_\sigma^2 e^{-ip \cdot x}. \end{aligned} \quad (\text{B2})$$

Appendix C: Ward-Takahashi identity for scale symmetry

The scale symmetry is also explicitly broken by the electromagnetic contribution and becomes anomalous. As a consequence, the isosinglet scalar can be coupled to the electromagnetic field via the scale anomaly arising from the quantum correction of the quark loop. To obtain the coupling form between the sigma field and the electromagnetic field, we consider the low-energy theorem related to the Ward-Takahashi identity for a photon two-point function coupled with the dilatation current j_D^μ ,

$$\lim_{q \rightarrow 0} \int d^4 y e^{iq \cdot y} \langle 0 | T \partial_\mu j_D^\mu(y) A_\mu(x) A_\nu(0) | 0 \rangle = i \delta_D \langle 0 | T A_\mu(x) A_\nu(0) | 0 \rangle \quad (\text{C1})$$

where δ_D denotes the infinitesimal scale transformation by the charge $Q_D = \int d^3 \vec{x} j_D^0(x)$, defined as $[iQ_D, \mathcal{O}(x)] = \delta_D \mathcal{O}(x) = (d_{\mathcal{O}} + x^\nu \partial_\nu) \mathcal{O}(x)$, for an operator \mathcal{O} with the scaling dimension $d_{\mathcal{O}}$.

Assuming the lightest scalar-meson pole-dominance, we can rewrite the left-hand side of Eq. (C1),

$$\lim_{q \rightarrow 0} \int d^4 y e^{iq \cdot y} \langle 0 | T \partial_\mu j_D^\mu(y) A_\mu(x) A_\nu(0) | 0 \rangle = -i \sqrt{\frac{N_f}{2}} f_\pi \lim_{q \rightarrow 0} \langle \sigma_0(q) | T A_\mu(x) A_\nu(0) | 0 \rangle. \quad (\text{C2})$$

Here, we have used the low energy theorem in Eq. (B2). Hence, the overlap amplitude of two photons associated with the isosinglet scalar state can be described by the scale transformation for the photon propagator,

$$\langle \sigma_0(q=0) | T A_\mu(x) A_\nu(0) | 0 \rangle = -\sqrt{\frac{2}{N_f}} \frac{1}{f_\pi} \delta_D \langle 0 | T A_\mu(x) A_\nu(0) | 0 \rangle. \quad (\text{C3})$$

By using Eq. (C3), we will find the coupling form between the sigma field and the electromagnetic field.

Appendix D: Scale-anomaly induced-tadpole term at finite temperature

The photon propagator gets the thermal quantum correction arising from the quark loop calculation with the dynamical quark mass m_{dyn} . Hence, the photon propagator no longer takes the Lorentz-covariant form, and then the polarization structure can be generally decomposed into the three independent components,

$$D_{\mu\nu}(K) = \frac{-i}{K^2 - \Pi_T} P_{\mu\nu} + \frac{-i}{K^2 - \Pi_L} Q_{\mu\nu} + (\xi - 1) \frac{i K_\mu K_\nu}{K^4}, \quad (\text{D1})$$

where the four-momentum of the photon denotes $K_\mu = (\omega, k_1, k_2, k_3)$. ξ is the gauge fixing parameter, and $P_{\mu\nu}$ and $Q_{\mu\nu}$ represent the transverse- and the longitudinal-polarization tensors,

$$\begin{aligned} P_{\mu\nu} &= \tilde{\eta}_{\mu\nu} + \frac{\tilde{K}_\mu \tilde{K}_\nu}{\tilde{k}^2}, \\ Q_{\mu\nu} &= \frac{-1}{K^2 \tilde{k}^2} \left(\vec{k}^2 u_\mu + \omega \tilde{K}_\mu \right) \left(\vec{k}^2 u_\nu + \omega \tilde{K}_\nu \right), \end{aligned} \quad (\text{D2})$$

with $\tilde{\eta}_{\mu\nu}$, \tilde{K}_μ and u_μ being

$$\begin{aligned} \tilde{\eta}_{\mu\nu} &= \text{diag}[0, -1, -1, -1], \\ \tilde{K}_\mu &= K_\mu - \omega u_\mu = (0, k_1, k_2, k_3), \\ u_\mu &= (+1, 0, 0, 0). \end{aligned} \quad (\text{D3})$$

The loop corrections $\Pi_{T,L}$ separately include the vacuum part $\Pi_{T,L}^{(T=0)}$ and thermal part $\Pi_{T,L}^{(\beta)}$,

$$\Pi_{T,L} = \Pi_{T,L}^{(T=0)} + \Pi_{T,L}^{(\beta)}. \quad (\text{D4})$$

At the one loop calculation performed by the dimensional regularization in $4 - \epsilon$ dimension, $\Pi_{T,L}$ are expressed as (for the detail of the thermal part, see [39, 40])

$$\begin{aligned} \Pi_T^{(T=0)} &= \Pi_L^{(T=0)} = -\frac{N_c}{2\pi^2} \sum_f Q_f^2 K^2 \int_0^1 dx x(1-x) \left(\frac{2}{\epsilon} - \log \{m_{\text{dyn}}^2 - x(1-x)K^2\} - \gamma + \log(4\pi) \right) \\ \Pi_T^{(\beta)} &= \frac{2N_c}{\pi^2} \sum_f Q_f^2 \left[\left\{ \frac{\omega^2}{\vec{k}^2} + \left(1 - \frac{\omega^2}{\vec{k}^2}\right) \ln \frac{\omega + |\vec{k}|}{\omega - |\vec{k}|} \right\} \right. \\ &\quad \times \left(\frac{m_{\text{dyn}}}{\beta} \tilde{a}(m_{\text{dyn}}\beta) - \frac{1}{\beta^2} \tilde{c}(m_{\text{dyn}}\beta) \right) + \frac{1}{8} \left\{ 2m_{\text{dyn}}^2 + \omega^2 + \frac{107\omega^2 - 131\vec{k}^2}{72} \right\} \tilde{b}(m_{\text{dyn}}\beta) \left. \right] \\ \Pi_L^{(\beta)} &= \frac{4N_c}{\pi^2} \sum_f Q_f^2 \left(1 - \frac{\omega^2}{\vec{k}^2}\right) \left[\left(1 - \frac{\omega}{2|\vec{k}|} \ln \frac{\omega + |\vec{k}|}{\omega - |\vec{k}|}\right) \left(\frac{m_{\text{dyn}}}{\beta} \tilde{a}(m_{\text{dyn}}\beta) - \frac{1}{\beta^2} \tilde{c}(m_{\text{dyn}}\beta) \right) \right. \\ &\quad \left. + \frac{1}{4} \left\{ 2m_{\text{dyn}}^2 - \omega^2 + \frac{11\vec{k}^2 + 37\omega^2}{72} \right\} \tilde{b}(m_{\text{dyn}}\beta) \right], \end{aligned} \quad (\text{D5})$$

where γ is the Euler-Mascheroni constant. $\tilde{a}(m_{\text{dyn}}\beta)$, $\tilde{b}(m_{\text{dyn}}\beta)$ and $\tilde{c}(m_{\text{dyn}}\beta)$ are given by

$$\begin{aligned} \tilde{a}(m_{\text{dyn}}\beta) &= \ln(1 + e^{-m_{\text{dyn}}\beta}), \\ \tilde{b}(m_{\text{dyn}}\beta) &= \sum_{n=1}^{\infty} (-1)^n \text{Ei}(-nm_{\text{dyn}}\beta) = \sum_{n=1}^{\infty} (-1)^n \left(-\int_{nm_{\text{dyn}}\beta}^{\infty} \frac{e^{-t}}{t} dt \right), \\ \tilde{c}(m_{\text{dyn}}\beta) &= \sum_{n=1}^{\infty} (-1)^n \frac{e^{-nm_{\text{dyn}}\beta}}{n^2}. \end{aligned} \quad (\text{D6})$$

With the above explicit expression, the scale transformation for the photon propagator showing up in Eq.(C3) is evaluated as

$$\begin{aligned} \delta_D D_{\mu\nu}(x) &= -\int \frac{d^4 p}{(2\pi)^4} \left[\left\{ F^{(T=0)}(K) + F_T^{(\beta)}(\omega, \vec{k}) \right\} \frac{i}{(K^2 - \Pi_T)^2} P_{\mu\nu} \right. \\ &\quad \left. + \left\{ F^{(T=0)}(K) + F_L^{(\beta)}(\omega, \vec{k}) \right\} \frac{i}{(K^2 - \Pi_L)^2} Q_{\mu\nu} \right] e^{-iK \cdot x}, \end{aligned} \quad (\text{D7})$$

where $F^{(T=0)}(K)$ and $F_{T,L}^{(\beta)}(\omega, \vec{k})$ represent the variation for the vacuum- and the thermal-parts, respectively. Actually, $F^{(T=0)}(K)$ is expressed as

$$F^{(T=0)}(K) = -2\frac{\beta(e)}{e} K^2 + \frac{N_c}{\pi^2} \sum_f Q_f^2 m_{\text{dyn}}^2 \left[-1 + \int_0^1 dx \frac{1}{1 - x(1-x)(K^2/m_{\text{dyn}}^2)} \right]. \quad (\text{D8})$$

The first term of the right hand side in Eq. (D8) induces the (local) tadpole interaction between the isosingle scalar and the electromagnetic fields. However, the second term corresponds to the nonlocal effective interaction, so that it does not contribute to the static effective potential describing the conventional chiral phase transition in the static picture.

$F_{T,L}^{(\beta)}(\omega, \vec{k})$ in Eq.(D7) gives the the thermal correction to the tadpole interaction, which is generated by the thermal mass of the electromagnetic field. Thus, we take the on-shell condition ($\omega = |\vec{k}|$) and the low energy limit ($\omega = |\vec{k}| \rightarrow 0$),

and then $F_{T,L}^{(\beta)}(\omega, \vec{k})$ goes like

$$\begin{aligned} \lim_{\omega=|\vec{k}| \rightarrow 0} F_T^{(\beta)}(\omega, \vec{k}) &= \sum_f Q_f^2 \frac{4N_c}{\pi^2} \left[\left(\frac{m_{\text{dyn}}}{\beta} \tilde{a}(m_{\text{dyn}}\beta) - \frac{1}{\beta^2} \tilde{c}(m_{\text{dyb}}\beta) \right) + \frac{1}{4} m_{\text{dyn}}^2 \tilde{b}(m_{\text{dyn}}\beta) \right] \\ &= \sum_f Q_f^2 F(\beta, m_{\text{dyn}}), \\ \lim_{\omega=|\vec{k}| \rightarrow 0} F_L^{(\beta)}(\omega, \vec{k}) &= 0. \end{aligned} \quad (\text{D9})$$

By picking up the relevant contributions to the effective potential, the scale transformation of the photon two-point function in Eq.(C3) is eventually evaluated as

$$\begin{aligned} \delta_D \langle 0|T A_\mu(x) A_\nu(0)|0\rangle &= - \int \frac{d^4 K}{(2\pi)^4} \left[\left\{ -2 \frac{\beta(e)}{e} K^2 + \sum_f Q_f^2 F(\beta, m_{\text{dyn}}) \right\} \frac{i}{(K^2 - \Pi_T)^2} P_{\mu\nu} \right. \\ &\quad \left. + \left\{ -2 \frac{\beta(e)}{e} K^2 \right\} \frac{i}{(K^2 - \Pi_L)^2} Q_{\mu\nu} \right] e^{-iK \cdot x}, \end{aligned} \quad (\text{D10})$$

where $Q_u = +2e/3$, $Q_d = -e/3$, $Q_s = -e/3$ and m_{dyn} is the dynamical quark mass generated by the spontaneous chiral symmetry breaking. Here, we have taken the flavor universal limit; $m_{\text{dyn}}^{(u)} = m_{\text{dyn}}^{(d)} = m_{\text{dyn}}^{(s)} = m_{\text{dyn}}$.

Now, we can read the effective interaction between the isosinglet scalar meson and the electromagnetic field at finite temperature, by using Eq. (C3) with Eq. (D10),

$$\mathcal{L}_{\text{int}}^{(\text{Tad})} = \frac{\beta(e)}{2e} \sqrt{\frac{2}{N_f} \frac{\sigma_0}{f_\pi}} F_{\mu\nu} F^{\mu\nu} - \frac{1}{2} \sum_f Q_f^2 F(T, m_{\text{dyn}}) \sqrt{\frac{2}{N_f} \frac{\sigma_0}{f_\pi}} A_\mu^{(T)} A_\mu^{(T)}, \quad (\text{D11})$$

where $A_\mu^{(T)}(x)$ represents the transversely polarized photon field,

$$A_\mu^{(T)}(x) = \int \frac{d^4 p}{(2\pi)^4} P_{\mu\nu}(p) A^\nu(p) e^{-ip \cdot x}. \quad (\text{D12})$$

At $T = 0$ the thermal part in the second term of Eq. (D11) vanishes. Then, we readily see that the effective interaction in Eq. (D11) surely reproduces the electromagnetic scale anomaly in the vacuum:

$$\langle 0 | \mathcal{L}_{\text{int}}^{(\text{Tad})} | 0 \rangle = \frac{\beta(e)}{2e} F_{\mu\nu} F^{\mu\nu}. \quad (\text{D13})$$

In the action level, the thermal part in Eq. (D11) can be rewritten as

$$\begin{aligned} \int d^4 x e^2 A_\mu^{(T)}(x) A_\mu^{(T)}(x) &= \int d^4 x e^2 \left[\int \frac{d^4 p}{(2\pi)^4} P_{\mu\nu}(p) A^\nu(p) e^{-ip \cdot x} \right] \left[\int \frac{d^4 q}{(2\pi)^4} P^{\mu\rho}(q) A_\rho(q) e^{-iq \cdot x} \right] \\ &= \int \frac{d^4 K}{(2\pi)^4} e^2 \frac{-1}{2k^2} \left\{ \int d^4 x \tilde{F}_{\sigma\rho}(x) e^{-iK \cdot x} \right\} \left\{ \int d^4 y \tilde{F}^{\sigma\rho}(y) e^{+iK \cdot y} \right\} \end{aligned} \quad (\text{D14})$$

where

$$\begin{aligned} \tilde{F}_{\sigma\rho}(x) &= \tilde{\partial}_\sigma \tilde{A}_\rho(x) - \tilde{\partial}_\rho \tilde{A}_\sigma(x), \\ \tilde{\partial}_\sigma &= \partial_\sigma - u_\sigma \partial_0 = (0, \partial_1, \partial_2, \partial_3), \\ \tilde{A}_\rho(x) &= \tilde{\eta}_{\rho\mu} A^\mu(x) = A_\rho(x) - A_0(x) u_\rho = (0, A_1, A_2, A_3). \end{aligned} \quad (\text{D15})$$

The thermal part in Eq.(D14) includes an infrared divergence. In a weak magnetic field regime ($\sqrt{eB} < T < m_{\text{dyn}}$) which we have focused on in the main text, the magnetic field strength $\tilde{F}_{12} = -B$ supplies the infrared cutoff, and should be implemented in Eq. (D14). Thus, the thermomagnetically induced tadpole can be evaluated as

$$\int d^4 x \left[-\frac{1}{2} \sum_f Q_f^2 F(T, m_{\text{dyn}}) \sqrt{\frac{2}{N_f} \frac{\sigma_0}{f_\pi}} A_\mu^{(T)} A_\mu^{(T)} \right] \approx \int d^4 x \left[\frac{1}{2e^2} \sum_f Q_f^2 F(T, m_{\text{dyn}}) \sqrt{\frac{2}{N_f} \frac{\sigma_0}{f_\pi}} eB \right]. \quad (\text{D16})$$

In total, the tadpole term generated in the effective potential takes the form

$$V_{\text{eff}}^{(\text{Tad})}(\bar{\sigma}_0) = -\sqrt{\frac{2}{N_f}} \frac{\sigma_0}{f_\pi} \left[\frac{\beta(e)}{e} B^2 + \frac{1}{2e^2} \sum_f Q_f^2 F(T, m_{\text{dyn}}) eB \right]. \quad (\text{D17})$$

Here, the magnetic effect is not taken into account when calculating the quark one-loop correction. This is because magnetic fields coming from the quark one-loop are subleading contributions in terms of powers of the magnetic field. As the magnetic field gets strong, the one-loop calculation depending the magnetic field should be taken into account. However, the dynamics of quarks are governed by the lowest Landau level states polarized along the direction parallel to the magnetic field, where the transverse part of the photon polarization does not couple to quarks. Thus, the tadpole term induced by the electromagnetic scale anomaly Eq. (D17) vanishes in the strong magnetic field regime, which is most eminent in the weak magnetic regime.

Appendix E: Effective potential based on quark-meson model

In this section, we show the effective potential based on the quark meson model. In the large N_c limit, the quantum correction to the effective potential only arises from the quark one-loop calculation regularized by the dimensional regularization, which consists of the vacuum part $V_{1\text{-loop}}^{\text{vac}}$ and the thermal part $V_{1\text{-loop}}^{\text{T}}$ [36]. By combining the quark parts with the mesonic part in Eq (A9) and the scale-anomaly induced-tadpole term in Eq. (2), the effective potential based on the quark-meson model is given as,

$$V_{\text{eff}}(\bar{\sigma}_0) = V_{\text{tree}}(\bar{\sigma}_0) + V_{1\text{-loop}}^{\text{vac}}(\bar{\sigma}_0) + V_{1\text{-loop}}^{\text{T}}(\bar{\sigma}_0) + V_{\text{eff}}^{(\text{Tad})}(\bar{\sigma}_0), \quad (\text{E1})$$

where

$$\begin{aligned} V_{1\text{-loop}}^{\text{vac}} &= +\frac{N_c m_{\text{dyn}}^4}{(4\pi)^2} \sum_f \left[\log \frac{\Lambda^2}{2|Q_f B|} + 1 \right] - \frac{N_c}{2\pi^2} \sum_f (Q_f B)^2 \left[\zeta^{(1,0)}(-1, x_f) + \frac{1}{2} x_f \log x_f \right] \\ V_{1\text{-loop}}^{\text{T}} &= -N_c \sum_f \frac{|Q_f B| T}{\pi^2} \int_0^\infty dp \left[\log \left\{ 1 + \exp \left(-\beta \sqrt{p^2 + (m_{\text{dyn}}^{(f)})^2} \right) \right\} \right. \\ &\quad \left. + 2 \sum_{n=1} \log \left\{ 1 + \exp \left(-\beta \sqrt{p^2 + (m_{\text{dyn}}^{(f)})^2 + 2n|Q_f B|} \right) \right\} \right], \end{aligned} \quad (\text{E2})$$

with $x_f = \left(m_{\text{dyn}}^{(f)} \right)^2 / (2|q_f B|)$. $\zeta(a, x)$ is the Hurwitz zeta-function, and Λ being the renormalization scale fixed as $\Lambda = 181.96 \text{ MeV}$ [36]. The dynamical quark masses is evaluated as

$$m_{\text{dyn}}^{(u)} = m_{\text{dyn}}^{(d)} = m_{\text{dyn}}^{(s)} = m_{\text{dyn}} = 2g\bar{\Phi}, \quad (\text{E3})$$

where g is the Yukawa coupling between the quarks and the mesonic sector. At $T = 0$ and $eB = 0$, we have set $m_{\text{dyn}} = 300 \text{ MeV}$.

Appendix F: Prediction to the order of chiral phase transition in three flavor symmetric limit from quark-meson model in a constant weak magnetic field

Beyond the chiral limit, we have also investigated the pion-mass (m_π) dependence on the chiral phase transition nature, in light of lattice simulations in the future. See Fig. 4, which corresponds to the $SU(3)$ flavor limit (the $N_f = 3$ diagonal line in Fig. 1). Varying m_π from zero, we observe a critical point, $m_\pi \simeq 80 \text{ MeV}$, at which the transition nature changes from the first order to the second order, and will then be the crossover as gets closer to the physical pion mass. This places another critical endpoint in the extended Columbia plot, in Fig. 1 (marked as the black circular blob).

The estimated value of the critical pion mass, $m_\pi \simeq 80 \text{ MeV}$, cannot be so serious, because the present model should include the model-systematic uncertainty, which may roughly be 30% when the values of T_c between ours and the lattice QCD result's are compared. See also footnote 3 in the main text.

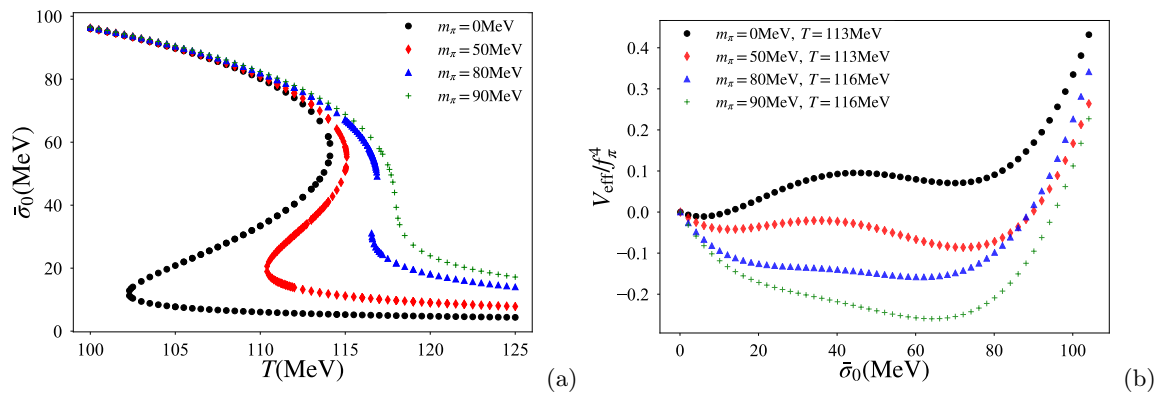


FIG. 4: Sensitivity of the pion mass to the chiral phase transition in the thermomagnetic QCD, predicted from the quark-meson model in the large N_c limit, for the $SU(3)$ flavor symmetric limit. Panel (a): The T -evolution of the chiral order parameter $\bar{\sigma}_0$. Panel (b): The corresponding deformation of the effective potential, normalized in a way similar to the ones in Figs. 2 and 3.

Existence of this another critical endpoint seems to be trivial, because the chiral crossover for the pion mass around the physical point has already been established on the lattice QCD in a strong magnetic field. In this sense, we have just confirmed that the extrapolation to a weaker magnetic field regime works fine, continuously leading to the second order from the crossover. Though being such trivial, this endpoint would also be deserved to explore on the lattice QCD in the future. In contrast, the critical endpoint claimed in the main text (in the m_s axis, arising as the interplay along the massless two and three flavor limits) is nontrivial due to the emergence of the dramatic change of the transition nature into the crossover (for two-flavor) from the first order (three-flavor).